Optics Letters

Temperature-compensated distributed hydrostatic pressure sensor with a thin-diameter polarization-maintaining photonic crystal fiber based on Brillouin dynamic gratings

LEI TENG,[1] HONGYING ZHANG,[2,4] YONGKANG DONG,[1,*] DENGWANG ZHOU,[1] TAOFEI JIANG,[1] WEI GAO,[2] ZHIWEI LU,[1] LIANG CHEN,[3] AND XIAOYI BAO[3]

[1]National Key Laboratory of Science and Technology on Tunable Laser, Harbin Institute of Technology, Harbin 150001, China
[2]Institute of Photonics and Optical Fiber Technology, Harbin University of Science and Technology, Harbin 150080, China
[3]Fiber Optics Group, Department of Physics, University of Ottawa, Ottawa K1N 6N5, Canada
[4]e-mail: zhy_hit@163.com
*Corresponding author: aldendong@gmail.com

Received 19 July 2016; revised 22 August 2016; accepted 24 August 2016; posted 26 August 2016 (Doc. ID 270886); published 15 September 2016

A temperature-compensated distributed hydrostatic pressure sensor based on Brillouin dynamic gratings (BDGs) is proposed and demonstrated experimentally for the first time, to the best of our knowledge. The principle is to measure the hydrostatic pressure induced birefringence changes through exciting and probing the BDGs in a thin-diameter pure silica polarization-maintaining photonic crystal fiber. The temperature cross-talk to the hydrostatic pressure sensing can be compensated through measuring the temperature-induced Brillouin frequency shift (BFS) changes using Brillouin optical time-domain analysis. A distributed measurement of hydrostatic pressure is demonstrated experimentally using a 4-m sensing fiber, which has a high sensitivity, with a maximum measurement error less than 0.03 MPa at a 20-cm spatial resolution.

OCIS codes: (190.2055) Dynamic gratings; (190.4370) Nonlinear optics, fibers; (290.5900) Scattering, stimulated Brillouin.

http://dx.doi.org/10.1364/OL.41.004413

Hydrostatic pressure measurement is necessary in a variety of areas [1]. Fiber Bragg gratings (FBGs)-based hydrostatic pressure sensors have been demonstrated in different configurations by calculating the wavelength shift of FBGs [2,3]. Hydrostatic pressure sensors based on interferometric and polarimetric sensors, like the Michelson interferometer, include a segment of high-birefringence microstructured fiber as the sensing element and codify the pressure on the transmission interference fringes changes measurement [4–7]. Varieties of specialty fibers, including polymer optical fiber [2,5], high-doped fibers [3], and photonic crystal fibers [4,6,7], offer new possibilities to enhance sensing measurement sensitivity for pressure detection. However, the disadvantage in these proposed techniques, such as FBGs and interferometers-based sensors, is the lack of distributed measurement ability.

Polarization-maintaining photonic crystal fiber (PM-PCF) has attracted considerable research interests for sensing applications [8–10]. Unlike the boron-doped stress-applying PMF, such as PANDA and Bow-tie, which have a higher thermal expansion coefficient of the core than that of the cladding; PM-PCFs are mostly made from pure silica and have significantly less temperature sensitivity on birefringence [8], so that they can provide less cross-sensitivity to temperature for sensing other parameters.

Brillouin scattering in optical fibers has been widely studied for distributed sensing applications and gained significant interests for the ability to monitor temperature and strain [11,12]. In recent years, the concept of Brillouin dynamic gratings (BDGs) has been reported [13–15] with many prominent advantages, and it was used intensively in all-optical information processing [16], light storage [17], microwave photonics [18], delay lines [19], optical spectrum analysis [20], and distributed sensing [21–25].

In this Letter, we propose and demonstrate a temperature-compensated distributed hydrostatic pressure sensor, for the first time to the best of our knowledge, based on BDGs with a thin-diameter pure silica PM-PCF. The hydrostatic pressure sensing is realized by measuring the birefringence changes through exciting and probing the BDGs; the temperature can be compensated by measuring the temperature-induced Brillouin frequency shift (BFS) through differential pulse-width pair Brillouin optical time-domain analysis (DPP-BOTDA) [12]. For the thin-diameter PM-PCF, the porous structure is more liable to be deformed and, subsequently, the birefringence change is more sensitive to hydrostatic pressure. The thermal expansion coefficients between the solid core and the porous cladding of the pure silica PM-PCF are approximately equal; therefore, there is a lower temperature birefringence coefficient, and the temperature cross-talk can be more accurately compensated. This novel distributed hydrostatic pressure sensor exhibits measurement errors of less than 0.03 MPa with a 20 cm spatial resolution.

BDGs can be generated as longitudinal acoustic waves through stimulated Brillouin scattering (SBS) in optical fibers, which has an optically refractive index modulated like FBGs [13–15,25]. Figure 1 illustrates the schematic diagram of excitation and readout of a BDG for distributed measurement of the birefringence of a PMF, where two counter-propagating pump waves, that is, pump 1 and pump 2, with a frequency offset equal to the BFS of the fiber, are launched into the x axis of the PMF. The BDG would be generated following the pump 1 pulse along the fiber through the SBS process. Meanwhile, a short probe pulse after pump 1 is injected immediately into the orthogonal y axis to interrogate the grating. A maximum reflection signal on the grating can be obtained when the frequency difference between the probe wave and pump 1, which propagates in the same direction as the probe wave, satisfies the phase matching condition [13–15]

$$\Delta v_{\text{Bire}} = \Delta n / n_g v, \tag{1}$$

where Δv_{Bire} is the birefringence-induced frequency shift (BireFS), Δn is the phase birefringence, n_g is the group refractive index, and v is the frequency of the probe wave. The BDGs spectrum can be obtained by recording the reflection signals while sweeping the optical frequency of the probe.

Figure 2 shows the experimental setup of the distributed hydrostatic pressure sensor. The output of a distributed feedback (DFB) laser at ∼1550 nm with a line width of <100 kHz is split into two arms by a 50/50 coupler, where one arm is used to supply pump 1 and the other for pump 2. A tunable laser with a wavelength resolution of 0.1 pm is used as the probe light. The Brillouin pump wave (pump 1) is generated with the original-frequency wave of the DFB laser and polarized to x-pol; a single-sideband modulator (SSBM) and a microwave synthesizer with an output frequency of 11.087 GHz are used to generate the Brillouin Stokes wave (pump 2), which is also polarized to x-pol. Two electro-optic modulators, EOM1 and EOM2, are used to generate the 20 ns square-shaped pump 1 pulse and 2 ns Gaussian-shaped probe pulse with a high extinction ratio larger than 40 dB. The pulsed pump 1 and probe are then combined in a 50/50 coupler and injected into the fiber under test (FUT). The power of the pump 1 pulse, the pump 2 pulse, and the probe pulses in the PM-PCF are about 300 mW, 2 mW, and 1.2 W, respectively. The reflection waves of the probe are received and recorded by a photodiode (PD) and data-acquisition (DAQ) card, with 2000 times averaging. The experimental setup we used has been proven in [25] to be an optimal choice for long-range and high-spatial-resolution

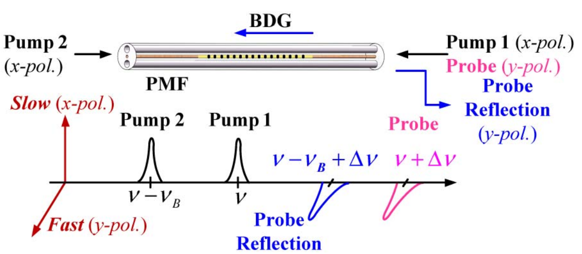

Fig. 1. Schematic diagram of the excitation and readout of a BDG.

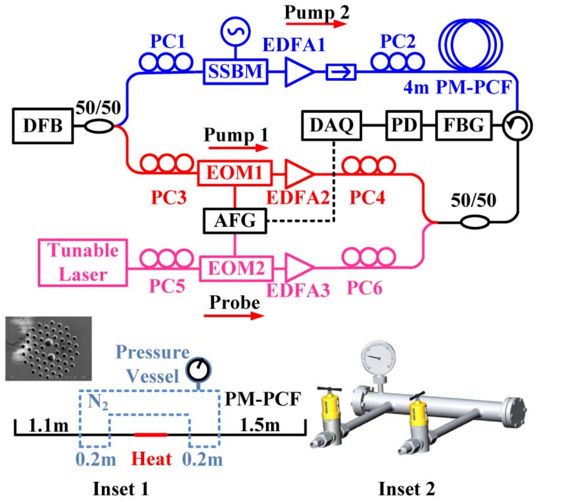

Fig. 2. Experimental setup of distributed hydrostatic pressure sensor. Inset 1: the structure of the FUT with a 20 cm heated section and two 20 cm pressurized sections and the sectional view of PM-PCF; inset 2: the self-designed pressure vessel.

distributed measurement of the birefringence of PMF without unwanted nonlinear effects and depletions.

The thin-diameter pure silica PM-PCF with a cladding of 99 μm used in our experiment has a mode-field diameter of 5.9 μm and measured BFSs of 11.087 GHz for the slow axis (x axis) and 11.084 GHz for the fast axis (y axis) at 1550 nm at 25°C obtained by a traditional BOTDA system [12]. In our experiment, the PM-PCF was divided into three parts, as shown in inset 1 of Fig. 2, with two 20 cm pressurized parts in a self-designed pressure vessel with a pressure resolution of 0.05 MPa (shown in inset 2 of Fig. 2) and a 20 cm heated part in a controllable oven with a temperature accuracy of 0.1°C. Due to the limitation of pressure-bearing capacity of our self-designed pressure vessel, the maximum applied pressure is ∼1.1 MPa.

The temperature and hydrostatic pressure properties of the BFS of the PM-PCF are investigated using the typical DPP-BOTDA [12] system, with a spatial resolution of 20 cm (40 ns/38 ns). Figure 3 illustrates the measured BFS results

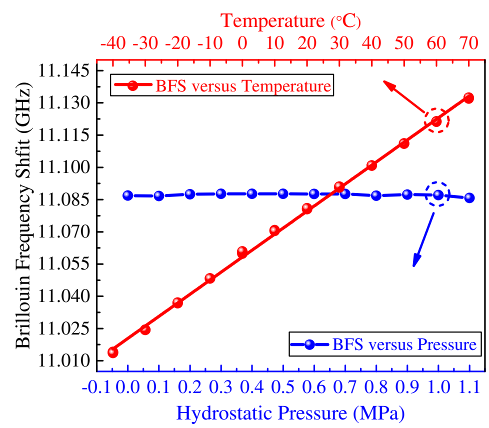

Fig. 3. Measured BFS results of PM-PCF at different temperatures (red spots) under a standard atmospheric pressure and at different hydrostatic pressures, 0–1.1 MPa (blue spots).

of FUT at different temperatures (red spots) under standard atmospheric pressure, ranging from −40°C to 70°C with a 10°C step, and under different hydrostatic pressures (blue spots), ranging from 0 to 1.1 MPa at room temperature (25°C). It is shown that the BFS moves toward a higher frequency as the temperature increases. The temperature dependence of BFS is obtained by linear fitting and a temperature coefficient for BFS C_B^T of 1.07 MHz/°C is obtained. It is indicated that the BFS of this kind of PM-PCF has a lower sensitivity to the hydrostatic pressure changes, with a BFS difference of only 1.88 MHz in the pressure ranges of 0 to 1.1 MPa.

Next, we investigated the temperature and hydrostatic pressure influences of the BireFS of the PM-PCF using the setup in Fig. 2. The temperature of the oven changes from −40°C to 70°C. We used other fibers outside of the oven, at the constant temperature of 25°C, as the reference for the compensation of the two laser frequency shift caused by a long-term working. At individual temperatures the frequency difference between pump 1 and pump 2 was adjusted to the appropriate BFS, according to the Fig. 3, to maximize the BDG reflection. The measured BireFS variations, with respect to different temperatures, are plotted in Fig. 4, from where it can be found that the BireFS difference is about 176 MHz for a temperature range of −40°C to 40°C, corresponding to 2.2 MHz/°C, and the BireFS difference is 24 MHz for temperatures from 40°C to 70°C, corresponding to 0.84 MHz/°C. The temperature birefringence coefficient for this PM-PCF is much smaller than that of PANDA, about −55.81 MHz/°C [21]. The characterization of the nonlinear temperature dependence of birefringence is mainly due to the effect of coating [22].

Distributed hydrostatic pressure sensing at different pressures has been characterized in two pressurized parts, Part A and Part B. The fitting results are shown in Fig. 5, with different pressures ranging from 0 to 1.05 MPa. From Fig. 5(a), it can be discovered that the birefringence increases with increasing pressures. The dark cyan curve is the measured result without any pressures, where the signal fluctuations indicate non-uniform birefringence over the fiber; the birefringence non-uniformity was also observed in other types of PMFs [21,25]. The BireFS difference, that is, hydrostatic pressure induced frequency shift, can be calculated by subtracting the initial frequency shift [the dark cyan curve in Fig. 5(a)], as shown in Fig. 5(b).

Figure 6 shows the linear dependence of the BireFS difference on the hydrostatic pressure of the PM-PCF in both Part A [Fig. 6(a)] and Part B [Fig. 6(b)], where the fitting results linearly illustrate the hydrostatic pressure sensitivities at 199 MHz/MPa for the two parts. In Fig. 5(b), the fiber part,

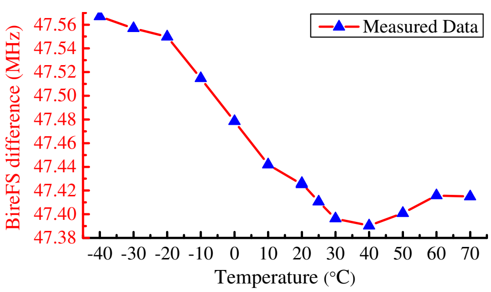

Fig. 4. Measured BireFS variations versus different temperatures.

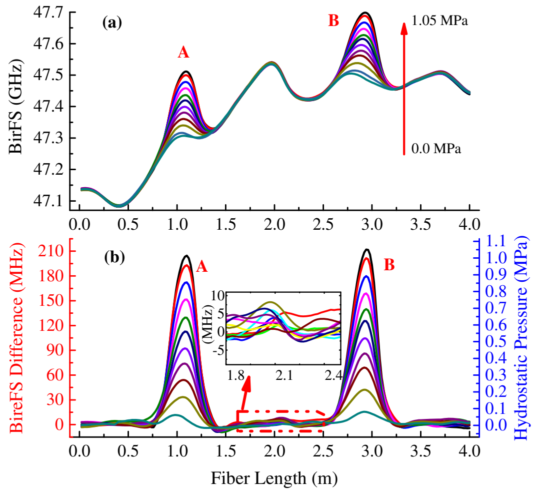

Fig. 5. Measured distributed BireFS results in the hydrostatic pressure range of 0–1.05 MPa, at 25°C and (b) BireFS difference corresponding to (a).

from 1.6 to 2.4 m, corresponds to the non-pressurized part, and we used the variation in the BireFS difference from this part to characterize the measurement standard deviation. As shown in the inset of Fig. 5(b), the measurement standard deviation is $\delta = \pm 5$ MHz, corresponding to a measurement error of 0.025 MPa.

According to the aforementioned results, the BFS of the fiber has a very low sensitivity to the hydrostatic pressure, so that the BFS change induced by pressure is neglected under 1.1 MPa in this experiment. To eliminate temperature cross-talk effects on the birefringence changes, the first step we conducted was to interrogate BFS changes by obtaining the temperature distribution over the FUT, and then BireFS changes of the FUT induced by both temperature and pressures were interrogated. Next, the effect on the fiber birefringence from the ambient temperature can be subtracted according to the measured temperature distribution. Consequently, the hydrostatic pressure-induced birefringence changes without temperature disturbance can be obtained.

The temperature measurement error of BOTDA is about ±0.5°C [12], which corresponds to temperature-induced BireFS changes of ±1.1 MHz for the PM-PCF we used and

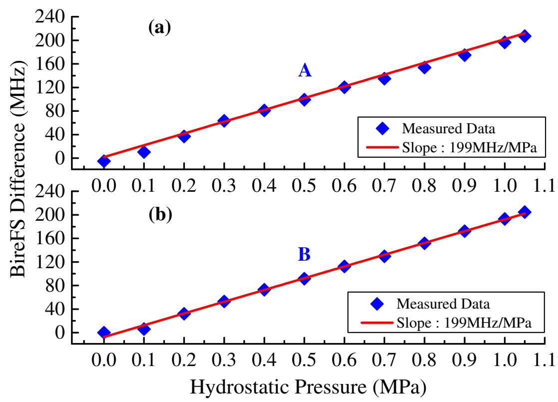

Fig. 6. BireFS differences versus different hydrostatic pressure for the two pressurized part, (a) Part A and (b) Part B.

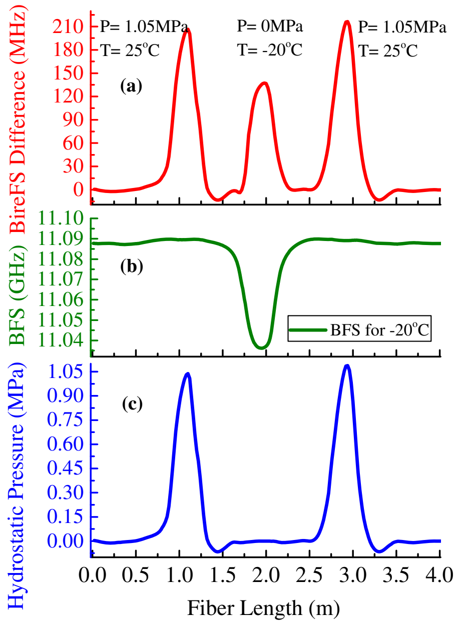

Fig. 7. (a) Simultaneously distributed hydrostatic pressure (1.05 MPa) and temperature (−20°C) measurements. (b) The BFS of the FUT at −20°C. (c) The measured hydrostatic pressure after compensating for the temperature cross-talk.

BireFS changes of ±27.5 MHz for PANDA [21]. From Fig. 6, it can be calculated that the BireFS changes at ±1.1 MHz are equivalent to a hydrostatic pressure change of 0.005 MPa; by contrast, the BireFS changes at ±27.5 MHz are equal to a hydrostatic pressure change of ±0.14 MPa. Therefore, the PM-PCF is preferable to compensate for the temperature changes and reduce the cross-talk to pressure measurement. Moreover, taking the error propagation from the BFS uncertainty of ±0.5°C [12] into consideration, the maximum measurement error should be modified to less than 0.03 MPa.

The BFS difference, $\Delta\nu_B$, and BireFS difference, $\Delta\nu_{\mathrm{Bire}}$, caused by temperature and pressure can be expressed as Eqs. (2) and (3):

$$\Delta\nu_B = C_B^T \Delta T + \Delta\nu_B^P, \tag{2}$$

$$\Delta\nu_{\mathrm{Bire}} = \Delta\nu_{\mathrm{Bire}}^T + C_{\mathrm{Bire}}^P \Delta P. \tag{3}$$

During the experiment, the FUT is under the loosen condition, which means the strain-induced BFS changes can be ignored. And the pressure-induced BFS changes, $\Delta\nu_B^P$, can also be ignored as mentioned. From the BOTDA data, the temperature-induced BFS changes, $C_B^T \Delta T$, can be obtained and the temperature changes can be computed. So the temperature-induced BireFS difference, $\Delta\nu_{\mathrm{Bire}}^T$, can be calculated according to Fig. 4. Finally, $\Delta\nu_{\mathrm{Bire}}^T$ can be subtracted, and the hydrostatic pressure, $C_{\mathrm{Bire}}^P \Delta P$, without temperature disturbance can be obtained.

Figure 7 indicates the process of measuring the hydrostatic pressure and compensating for the temperature cross-talk. Figure 7(a) shows the simultaneous hydrostatic pressure (1.05 MPa) and temperature (−20°C) measurements based on BDG. With the DPP-BOTDA system, the temperature of −20°C is effectively discriminated, as shown in Fig. 7(b). The measured hydrostatic pressure after the compensating temperature cross-talk is shown in Fig. 7(c). The results shown in Fig. 7 are consistent with the results in Figs. 4 and 5.

To conclude, we have proposed and experimentally demonstrated a temperature-compensated distributed hydrostatic pressure sensor based on BDG with the thin-diameter pure silica PM-PCF as the FUT. The temperature-induced BFS and BireFS have been used to calculate and compensate for the temperature cross-talk for hydrostatic pressuring sensing. The optimal experimental scheme with a continue wave (CW) pump 1, a long pump 2 pulse, and a short probe pulse is adopted to avoid unwanted nonlinear effects and pump depletion, consequently enhancing the measurement accuracy. The sensing technique features a distributed measurement, temperature compensation, and a high sensitivity to hydrostatic pressure, with a maximum measurement error of less than 0.03 MPa at a spatial resolution of 20 cm.

Funding. 863 Program of China (2014AA110401); National Key Technology Research and Development Program of the Ministry of Science and Technology of China (2014BAG05B07); National Key Scientific Instrument and Equipment Development Project (2013YQ040815); National Science Foundation (NSF) (61575052, 61308004); Foundation for Talents Returning from Overseas of Harbin (2013RFLXJ013); Scientific Research Fund of Heilongjiang Provincial Education Department (12531093, ZD201415).

REFERENCES

1. G. K. Batchelor, *An Introduction to Fluid Dynamics* (Cambridge University, 2000).
2. K. Bhowmik, G. D. Peng, and Y. Luo, J. Lightwave Technol. **33**, 2456 (2015).
3. L. Jin, Z. Quan, L. Cheng, and B. O. Guan, J. Lightwave Technol. **31**, 1488 (2013).
4. F. C. Fávero, S. M. M. Quintero, C. Martelli, A. Silva, and I. C. S. Carvalho, Sensors **10**, 9698 (2010).
5. T. Martynkien, G. Wojcik, P. Mergo, and W. Urbanczyk, Opt. Express **40**, 3033 (2015).
6. M. K. Szczurowski, T. Martynkien, and G. Statkiewicz-Barabach, Opt. Express **18**, 12076 (2010).
7. K. Tarnowski, A. Anuszkiewicz, and J. Olszewski, Opt. Lett. **38**, 5260 (2013).
8. X. Y. Dong, H. Y. Tam, and P. Shum, Appl. Phys. Lett. **90**, 131 (2007).
9. H. Y. Fu, A. C. L. Wong, P. A. Wong, P. A. Childs, H. Y. Tam, Y. B. Liao, C. Lu, and P. K. A. Wai, Opt. Express **17**, 18501 (2009).
10. B. Dong, D. P. Zhou, and L. Wei, J. Lightwave Technol. **28**, 1011 (2010).
11. Y. Mizuno, N. Hayashi, H. Fukuda, K. Y. Song, and K. Nakamura, Light Sci. Appl. **5**, e16184 (2016).
12. X. Bao and L. Chen, Sensors **11**, 4152 (2011).
13. K. Y. Song, W. Zou, and Z. He, Opt. Lett. **33**, 926 (2008).
14. Y. K. Dong, L. Chen, and X. Bao, Opt. Express **18**, 18960 (2010).
15. Y. K. Dong, L. Chen, and X. Bao, Opt. Lett. **35**, 193 (2010).
16. M. Santagiustina, S. Chin, N. Primerov, L. Ursini, and L. Thévenaz, Sci. Rep. **3**, 1594 (2013).
17. H. G. Winful, Opt. Express **21**, 10039 (2013).
18. J. Sancho, N. Primerov, and S. Chin, Opt. Express **20**, 6157 (2012).
19. S. Chin and L. Thévenaz, Laser Photon. Rev. **6**, 724 (2012).
20. Y. Dong, T. F. Jiang, and L. Teng, Opt. Lett. **39**, 2967 (2014).
21. W. Zou, Z. He, and K. Hotate, Opt. Express **17**, 1248 (2009).
22. Y. H. Kim and K. Y. Song, J. Lightwave Technol. **33**, 4922 (2015).
23. K. Y. Song and H. J. Yoon, Opt. Lett. **35**, 52 (2010).
24. K. Y. Song, Opt. Express **20**, 27377 (2012).
25. Y. Dong, H. Zhang, Z. Lu, and X. Bao, J. Lightwave Technol. **31**, 2681 (2013).